Convection in nanofluids with a particle-concentration-dependent thermal conductivity

Martin Glässl, Markus Hilt, and Walter Zimmermann*
Theoretische Physik I, Universität Bayreuth, DE-95440 Bayreuth, Germany
(Received 16 September 2010; revised manuscript received 9 March 2011; published 26 April 2011)

Thermal convection in nanofluids is investigated by means of a continuum model for binary-fluid mixtures, with a thermal conductivity depending on the local concentration of colloidal particles. The applied temperature difference between the upper and the lower boundary leads via the Soret effect to a variation of the colloid concentration and, therefore, to a spatially varying heat conductivity. An increasing difference between the heat conductivity of the mixture near the colder and the warmer boundary results in a shift of the onset of convection to higher values of the Rayleigh number for positive values of the separation ratio $\psi > 0$ and to smaller values in the range $\psi < 0$. Beyond some critical difference of the thermal conductivity between the two boundaries, we find an oscillatory onset of convection not only for $\psi < 0$, but also within a finite range of $\psi > 0$. This range can be extended by increasing the difference in the thermal conductivity, and it is bounded by two codimension-2 bifurcations.

DOI: 10.1103/PhysRevE.83.046315 PACS number(s): 47.55.P−, 47.57.E−, 44.10.+i

I. INTRODUCTION

Thermal convection plays a central role in geophysics [1,2], atmospheric dynamics [3], and various technical applications, whereof nanofluids were recently identified as efficient heat-transfer substances [4–7]. Rayleigh-Bénard convection with its numerous variants is also a classical laboratory experiment for studying generic phenomena of nonlinear dynamics and pattern formation, which occur in this system as in several other fields of natural science [2,8–10]. In most of the related theoretical studies, the Oberbeck-Boussinesq (OB) approximation for thermal convection is used, where constant material parameters independent of the thermodynamic variables are assumed, except the temperature-dependent density within the buoyancy term, which is the essential driving force of convection.

Non-Boussinesq contributions to the governing equations for convective systems are often required to model various phenomena in an appropriate way. Around 4 °C, for instance, the linear term in the thermal expansion of water vanishes and the quadratic contribution has to be taken into account. It is well known that this modification changes the symmetry condition in a thin fluid layer heated from below, leading to hexagonal convection patterns instead of stripe patterns close to the onset of convection [8,11]. Strongly varying material properties in the Earth's mantle are a major motivation for using a temperature-dependent viscosity in models of thermal convection in single component fluids, which is another non-Boussinesq contribution [12–17]. A further example is a temperature-dependent thermal conductivity, being considered to be important, for instance, for explaining a delayed cooling of the Earth's mantle [18]. There are also recent studies about non-Boussinesq contributions to convection in binary-fluid mixtures where either a temperature-dependent thermodiffusion coefficient or a dependence of the viscosity on the local composition was taken into account [19–21].

Convection in binary-fluid mixtures is another classical, driven pattern-forming system [22,23], which has attracted wide attention during the last decades [22–30]. In binary-fluid mixtures, the concentration field of one of the two constituents enters the basic equations as an additional dynamic quantity [22–24]. Via the Soret effect (*thermophoresis*), a temperature gradient, which is applied vertically across a convection cell, may cause variations of the concentration field that couples into the Navier-Stokes equations for the velocity field via the buoyancy term. Depending on the sign of the Soret effect, the heavier constituent is either driven to the colder upper boundary or to the warmer lower boundary. In the former case, one obtains stationary convection patterns near the onset of convection, and in the latter case oscillatory patterns. Experimentally, the onset of convection is well investigated in mixtures of alcohol and water as well as for ^{3}He/^{4}He mixtures [8]. The possibility of having both a stationary as well as an oscillatory onset of convection, including a so-called codimension-2 bifurcation at the transition point, made it a very attractive model system for generic bifurcation phenomena [8,31].

Colloidal suspensions, also known as nanofluids, may be considered as a further example of a binary mixture, with the suspended particles being the second constituent. Recently, convection in colloidal suspensions [32–36] has been investigated experimentally with a special focus on Soret driven convection [32–34], on bistable heat transfer that is caused by sedimentation effects [35], or on the effects of thermosensitive particles [36].

Additionally, in several nanofluids with particle sizes in the range of 1–100 nm, a strong dependence of the thermal conductivity on the concentration of nanoparticles was reported (see, e.g., Refs. [4,6,7,37–39]). This dependence presents another non-Boussinesq effect. In this paper, we investigate its impact on the onset of convection. Taking the particle-concentration-dependent thermal conductivity into account, we go beyond other recent studies with the focus on convection in colloidal suspensions [40,41], where the Boussinesq approximation has been used.

The enhancement of the thermal conductivity in fluids by increasing the concentration of suspended nanoparticles was confirmed by a recent benchmark study with contributions of more than 30 researchers [6]. Despite the promising

*walter.zimmermann@uni-bayreuth.de

applications of nanofluids for improving heat transfer in cooling systems, a considerable number of open questions are left. Among several possible transport phenomena, discussed to explain the heat-transfer enhancement in nanofluids, Brownian diffusion and thermophoresis were identified as the two most important ones [5]. Both mechanisms build the crucial extensions from models for a single component Newtonian fluid to models for convection in binary-fluid mixtures [22,24].

This paper is organized as follows: In Sec. II, we briefly present the underlying equations of motion and introduce a linear relation between the heat conductivity and the particle concentration, which leads to a nonlinear spatial dependence of the heat conductive state. The essential methods of the linear stability analysis for the determination of the onset of convection are presented in Sec. III. Our numerical results for the onset of convection include a prediction of an oscillatory onset even in the range of positive values of the separation ratio for both cases, no-slip boundary conditions in Sec. III A, and free-slip boundary conditions in Sec. III B. In Sec. IV, we summarize and discuss our results.

II. BASIC EQUATIONS AND HEAT CONDUCTIVE STATE

To describe convection in a horizontal layer of a colloidal suspension, the common mean field approach for binary-fluid mixtures is used [22,25,26,29,30,42]. In addition, we take into account a linear dependence of the thermal conductivity κ on the mass fraction of the colloidal particles $N(\mathbf{r},t)$. The mass density of the colloidal particles ρ_c is assumed to be similar to the mass density of the solvent ρ_s, i.e., $\varepsilon = \rho_c/\rho_s \simeq 1$. Furthermore, we assume small colloidal particles undergoing strong Brownian motion, so that sedimentation effects become negligible. Deviations of $N(\mathbf{r},t)$ from the mean mass fraction N_0 may lead to a spatial dependence of the thermal conductivity via the linear relation

$$\kappa = \kappa_0 \left[1 + \gamma (N - N_0)\right], \tag{1}$$

where κ_0 describes the mean thermal conductivity of the suspension and $\gamma = (1/\kappa_0)\,\partial\kappa/\partial N$ is a measure for the dependence of the thermal conductivity on the concentration of the nanoparticles. Heat conduction experiments with small volume fractions of nanoparticles match with the assumption $\gamma \sim 2.5$ [6,37,38].

The common set of basic transport equations for incompressible binary-fluid mixtures (cf. Refs. [22,25,26,29,30]) involves the temperature field $T(\mathbf{r},t)$, the mass fraction of the particles $N(\mathbf{r},t)$, the fluid velocity $\mathbf{v}(\mathbf{r},t)$, the density of the mixture $\rho(\mathbf{r},t)$, and the pressure field $p(\mathbf{r},t)$:

$$\boldsymbol{\nabla}\cdot\mathbf{v} = 0\,, \tag{2a}$$

$$(\partial_t + \mathbf{v}\cdot\boldsymbol{\nabla})\,T = \boldsymbol{\nabla}\cdot(\chi\boldsymbol{\nabla}T)\,, \tag{2b}$$

$$(\partial_t + \mathbf{v}\cdot\boldsymbol{\nabla})\,N = D\,\boldsymbol{\nabla}\cdot\left(\boldsymbol{\nabla}N + \frac{k_T}{T}\,\boldsymbol{\nabla}T\right), \tag{2c}$$

$$(\partial_t + \mathbf{v}\cdot\boldsymbol{\nabla})\,\mathbf{v} = -\frac{1}{\rho_0}\,\boldsymbol{\nabla}p + \nu\,\Delta\mathbf{v} + \frac{\rho}{\rho_0}\,\mathbf{g} \tag{2d}$$

Equation (2a) describes the incompressibility of the fluid. $\chi = \kappa/\rho_0$ in the heat equation (2b) denotes the thermal diffusivity of the mixture, which is in our model a function of the concentration of the suspended colloids. D in Eq. (2c) is the diffusion constant, which takes (due to the size of the colloidal particles) much smaller values than in molecular binary-fluid mixtures. The dimensionless thermal-diffusion ratio k_T representing the cross coupling between the temperature gradient and the particle flux is related to the Soret coefficient S_T via $k_T/T = N(1-N)S_T$, which can be either positive or negative. Throughout this paper, $k_T/T \simeq N_0(1-N_0)S_T$ is regarded as constant. ν in the Navier-Stokes equations (2d) is the kinematic viscosity. The gravity field $\mathbf{g} = -g\mathbf{e}_z$ is chosen parallel to the z direction.

For the local density ρ of the suspension, we use a linearized equation of state [22,43]

$$\rho = \rho_0[1 - \alpha(T - T_0) + \beta(N - N_0)]\,, \tag{3}$$

with the thermal expansion coefficient $\alpha = -(1/\rho_0)\partial\rho/\partial T$ and $\beta = (1/\rho_0)\partial\rho/\partial N$ reflecting the density contrast between the solvent and the suspended particles. According to the Boussinesq approximation, this dependence of the density is taken into account only within the buoyancy term. The sign of β indicates whether the colloidal particles have a higher or a lower mass density compared to the solvent. Here, we assume $\beta > 0$ corresponding to $\varepsilon \gtrsim 1$.

Boundary conditions. The fluid layer is confined between two impermeable, parallel plates at a distance d, and extends infinitely in the x-y plane. The lower plate at $z = -d/2$ is kept at a higher temperature $T_0 + \delta T/2$ than the upper plate at $z = +d/2$, with the lower temperature $T_0 - \delta T/2$. Together with a vanishing mass current at the boundaries and realistic no-slip conditions for the flow field, we have the following set of boundary conditions at $z = \pm d/2$:

$$T = T_0 \mp \frac{\delta T}{2}\,, \tag{4a}$$

$$0 = \partial_z N + \frac{k_T}{T_0}\partial_z T, \tag{4b}$$

$$0 = v_x = v_y = v_z = \partial_z v_z\,. \tag{4c}$$

For geophysical applications, free-slip boundary conditions

$$0 = \partial_z v_x = \partial_z v_y = v_z = \partial_z^2 v_z \tag{5}$$

for the flow field are often considered to be more realistic [44]. In the case of a constant thermal conductivity and free-slip, permeable boundary conditions, an analytical determination of the onset of convection is possible [25]. By introducing a concentration-dependent thermal conductivity, this advantage is lost and one has to rely on numerical methods.

A. Heat conductive state

Together with the concentration-dependent heat conductivity given by Eq. (1), the constant vertical heat current $j_z = -\chi\,\partial_z T_{\mathrm{cond}}$ leads to a nonlinear z dependence of the time-independent temperature distribution $T_{\mathrm{cond}}(z)$ and the corresponding concentration distribution $N_{\mathrm{cond}}(z)$ of the heat conductive state. Both are derived in the Appendix and are of the form

$$T_{\mathrm{cond}} = T_0 + \frac{\delta T}{\xi}\left(\frac{1}{2}[1 + Y(\xi)] - W(z,\xi)\right) \tag{6a}$$

$$= T_0 - \delta T\,\frac{z}{d} - \xi\,\frac{\delta T}{2}\left(\frac{1}{4} - \frac{z^2}{d^2}\right) + \mathcal{O}(\xi^2) \quad (6b)$$

$$N_{\rm cond} = N_0 + \frac{\delta N}{\xi}[1 - W(z,\xi)] \quad (6c)$$

$$= N_0 - \delta N\,\frac{z}{d} - \xi\,\frac{\delta N}{2}\left(\frac{1}{12} - \frac{z^2}{d^2}\right) + \mathcal{O}(\xi^2)\,, \quad (6d)$$

with the abbreviations

$$W(z,\xi) = \sqrt{\xi[1 + Y(\xi)]\frac{z}{d} + \frac{1}{2}\left(1 + Y(\xi) + \frac{1}{3}\xi^2\right)}\,, \quad (7a)$$

$$Y(\xi) = \sqrt{1 - \frac{1}{3}\xi^2}\,, \qquad \xi = \gamma\, k_T\,\frac{\delta T}{T_0} \quad (7b)$$

and

$$\delta N = -\frac{k_T}{T_0}\,\delta T\,. \quad (7c)$$

For finite values of γ, the vertical heat current

$$j_z = \frac{\chi_0 \delta T}{2d}\left(1 + \sqrt{1 - \frac{1}{3}\xi^2}\right) \quad (8)$$

is reduced compared to the situation of a constant heat conductivity being independent of the particle concentration.

We would like to stress that Eqs. (6) are derived under the assumption of small values of δN, but these formulas are still reasonable for values up to $\delta N < N_0/3$. The restriction $|\xi| < \sqrt{3}$ according to Eq. (7b) has the same origin and is fulfilled by all parameters chosen in this work. For stronger variations of δN, the assumption of a constant thermodiffusion coefficient $k_T/T \simeq N_0(1 - N_0)S_T$ is not justified anymore and a generalized approach has to be chosen.

B. Dimensionless equations of convective fluid motion

For the further analysis, it is convenient to separate the basic heat conductive state in Eq. (6) from convective contributions as follows: $T(\mathbf{r},t) = T_{\rm cond}(z) + T_1(\mathbf{r},t)$ and $N(\mathbf{r},t) = N_{\rm cond}(z) + N_1(\mathbf{r},t)$. By using the rotational symmetry in the fluid layer, we can restrict our analysis to two spatial dimensions, namely, to the x-z plane. With this simplification, the fluid velocity $\mathbf{v} = (v_x,0,v_z)$ can be expressed by a *stream function* $\phi(x,z,t)$:

$$v_z = \partial_x \phi, \quad v_x = -\partial_z \phi\,. \quad (9)$$

Subsequently, all lengths are scaled by the vertical distance d and times by the vertical thermal-diffusion time d^2/χ_0. By scaling the temperature field T by $(\chi_0\nu_0)/(\alpha g d^3)$, the concentration field N by $-(k_T\chi_0\nu_0)/(T_0\alpha g d^3)$, and the stream function ϕ by $\chi_0 d$, we are left with five dimensionless parameters: The *Rayleigh number* R, the *Prandtl number* P, the *Lewis number* L, and the *separation ratio* ψ,

$$P = \frac{\nu_0}{\chi_0}, \quad L = \frac{D}{\chi_0}, \quad R = \frac{\alpha g d^3}{\chi_0\nu_0}\,\delta T, \quad \psi = \frac{\beta k_T}{\alpha T_0}\,, \quad (10)$$

are well known from molecular binary-fluid mixtures [26,29]. The fifth dimensionless quantity

$$\zeta = \gamma\,\frac{\nu_0\chi_0}{g\beta d^3} \quad (11)$$

is introduced to characterize the spatially varying contribution to the thermal diffusivity caused by the concentration dependence of the thermal conductivity of the suspension. An illustration of its physical meaning is obtained by considering the thermal conductivity contrast between the upper and the lower boundary

$$\tilde{\kappa} = \frac{1 + \frac{1}{2}\gamma\, k_T\, \delta T/T_0}{1 - \frac{1}{2}\gamma\, k_T\, \delta T/T_0} = \frac{1 + \frac{1}{2}\,R\,\psi\,\zeta}{1 - \frac{1}{2}\,R\,\psi\,\zeta}\,, \quad (12)$$

which is essentially a function of the product of the three dimensionless control parameters $R\,\psi\,\zeta = \xi$.

In the following, we will discuss our results essentially in dependence on ψ and ζ, whereas P and L are considered as constants.

Introducing a rescaled temperature deviation $\theta = (R/\delta T)\,T_1$, a rescaled concentration deviation $\tilde{N}_1 = -(T_0 R/k_T \delta T)N_1$, and a rescaled stream function $\Phi = 1/(\chi_0 d)\,\phi$ in terms of these dimensionless quantities and using the combined function $\tilde{c} = \tilde{N}_1 - \theta$ instead of $\tilde{N}_1$, we obtain

$$\begin{aligned}&\partial_t\theta - W_0\Delta\theta - R\psi\zeta\,W_1(\partial_z c + 2\partial_z\theta) - W_2(c+\theta) - RW_1\partial_x\Phi\\ &\quad = -\psi\zeta[(\partial_x\theta)\partial_x(\theta+c) + (\partial_z\theta)\partial_z(\theta+c) + \Delta\theta(\theta+c)]\\ &\qquad + (\partial_z\Phi\partial_x - \partial_x\Phi\partial_z)\,\theta\,, \quad (13a)\\ &\partial_t c + W_0\Delta\theta + R\,\psi\,\zeta\,W_1(\partial_z c + 2\partial_z\theta) + W_2(c+\theta) - L\Delta c\\ &\quad = +\psi\zeta[(\partial_x\theta)\partial_x(\theta+c) + (\partial_z\theta)\partial_z(\theta+c) + \Delta\theta(\theta+c)]\\ &\qquad + (\partial_z\Phi\partial_x - \partial_x\Phi\partial_z)\,c\,, \quad (13b)\\ &\partial_t\Delta\Phi - P\Delta^2\Phi - P(1+\psi)\partial_x\theta - P\psi\partial_x c\\ &\quad = P(\partial_z\Phi\partial_x - \partial_x\Phi\partial_z)\,\Delta\Phi\,, \quad (13c)\end{aligned}$$

with the abbreviations

$$W_0 = W(z,\xi)\,, \quad (14a)$$

$$W_1 = \frac{1}{\xi}\partial_z W(z,\xi)\,, \quad (14b)$$

$$W_2 = \partial_z^2 W(z,\xi)\,. \quad (14c)$$

For reasons of simplicity, all the tildes have been suppressed. No-slip, impermeable boundary conditions for the fields θ, c, and Φ demand

$$\theta = \partial_z c = \Phi = \partial_z\Phi = 0 \quad \text{at } z = \pm\tfrac{1}{2}, \quad (15)$$

while free-slip, permeable boundary conditions [25,42]

$$\theta = c = \Phi = \partial_z^2\Phi = 0 \quad \text{at } z = \pm\tfrac{1}{2}\,. \quad (16)$$

In this paper, we present both results based upon no-slip, impermeable boundary conditions and those based upon free-slip, permeable boundary conditions.

III. LINEAR STABILITY OF THE HEAT CONDUCTIVE STATE AND ONSET OF CONVECTION

To determine the parameters at the onset of convection, we investigate the linear stability of the heat conductive state given by Eqs. (6) with respect to small perturbation fields: $\theta(x,z,t)$, $c(x,z,t)$, and $\Phi(x,z,t)$. The reduced set of three linear partial

differential equations (PDEs) with constant coefficients may be solved by the ansatz

$$\begin{pmatrix} \theta(x,z,t) \\ c(x,z,t) \\ \Phi(x,z,t) \end{pmatrix} = \mathbf{u}_0(z) e^{iqx} e^{\sigma t} + \text{c.c.} \tag{17}$$

with the vector function

$$\mathbf{u}_0(z) = \begin{pmatrix} \bar{\theta}(z) \\ \bar{c}(z) \\ \bar{\Phi}(z)/(iq) \end{pmatrix} \tag{18}$$

and c.c. denoting the complex conjugate, leading to a boundary eigenvalue problem with respect to z and the eigenvalue σ. We solve the remaining linear ordinary differential equations (ODEs) by two different methods, as summarized in the following paragraphs.

The first one is the standard *shooting method* as described in detail for binary-fluid convection in Ref. [29]. The resulting coupled ODEs for the components of the vector function $\mathbf{u}_0(z)$ are integrated for a set of initial conditions at one boundary. With the value of $\mathbf{u}_0$ at the opposite boundary, a determinant $f(\sigma,R,q,Q,P,L,\psi)$ follows. Keeping the initial conditions fixed, either R or σ are varied such that f vanishes. The resulting values of σ and R are functions of the remaining parameters.

The second approach is based upon the so-called *Galerkin method*. The components of $\mathbf{u}_0(z)$ are expanded with respect to a suitable chosen set of functions fulfilling already the boundary conditions, i.e., either Eqs. (15) or (16). Examples for this alternative numerical method may be found in Refs. [45–47]. The resulting generalized algebraic eigenvalue problem is solved numerically.

At the onset of convection, the small perturbations θ, c, and Φ neither grow nor decay. This is the so-called neutral stability condition, where the real part $\text{Re}(\sigma)$ of the eigenvalue σ with the largest real part (fastest growing mode) vanishes:

$$\text{Re}(\sigma) = 0 \quad \text{with} \quad \sigma = \sigma(R,q,\zeta,P,L,\psi)\,. \tag{19}$$

This yields the Rayleigh number

$$R_0(q) = R_0(q,\zeta,P,L,\psi) \tag{20}$$

as a function of the chosen wave number q and describes the so-called *neutral curve* with a minimum at the critical wave number q_c and the critical Rayleigh number $R_c = R_0(q_c)$. Convection sets in with a wave number $q \simeq q_c$ by crossing R_c from below. Depending on parameters, the onset of convection may take place via a *stationary bifurcation* with a vanishing imaginary part of the eigenvalue $\text{Im}(\sigma) = 0$, or via a *Hopf bifurcation* with a finite Hopf frequency $\text{Im}(\sigma) = \pm\omega_0(q,\zeta,P,L,\psi)$ with its critical value $\omega_c = \omega_0(q_c)$.

Throughout this paper, we choose for reasons of simplicity the Prandtl number $P = 10$. Since nanoparticles are much larger than, for instance, alcohol molecules in water, their mass diffusion is more than two orders of magnitude smaller. Accordingly, the Lewis number in nanofluids takes considerably smaller values of about $L = 10^{-4}$ [48]. Growing linearly with the particle's size [48], the Soret effect can be changed in a wide range by varying the mass density with respect to the base fluid or the particle diameter. For small nanoparticles in water $\zeta \simeq 0.01$ and in glycerin $\zeta \simeq 10$ are appropriate values.

A. No-slip, impermeable boundary conditions

It is a major result of this work that a particle-concentration-dependent thermal conductivity, described by finite values of ζ, leads in the range $\psi > 0$ to a shift of the onset of convection to larger values of R_c. As another important result, we find in the range $\psi \simeq L$ and beyond some critical value ζ_c an exchange of instabilities from a stationary bifurcation to an oscillatory one, and we characterize this transition as a function of ψ and ζ.

The neutral curve $R_0(q)$ belonging to the lowest bifurcation from the heat conductive state at different values of ζ is shown in Figs. 1 and 2 for two representative positive values of the separation ratio ψ, namely, for $\psi = 10^{-5} \ll L$ (Fig. 1) and $\psi = 10^{-4} = L$ (Fig. 2). In both figures, the black solid line describes the neutral curve $R_0(q)$ corresponding to molecular binary fluids, i.e., $\zeta = 0$. It is included for illustrating the relative changes of the neutral curve as a function of ζ.

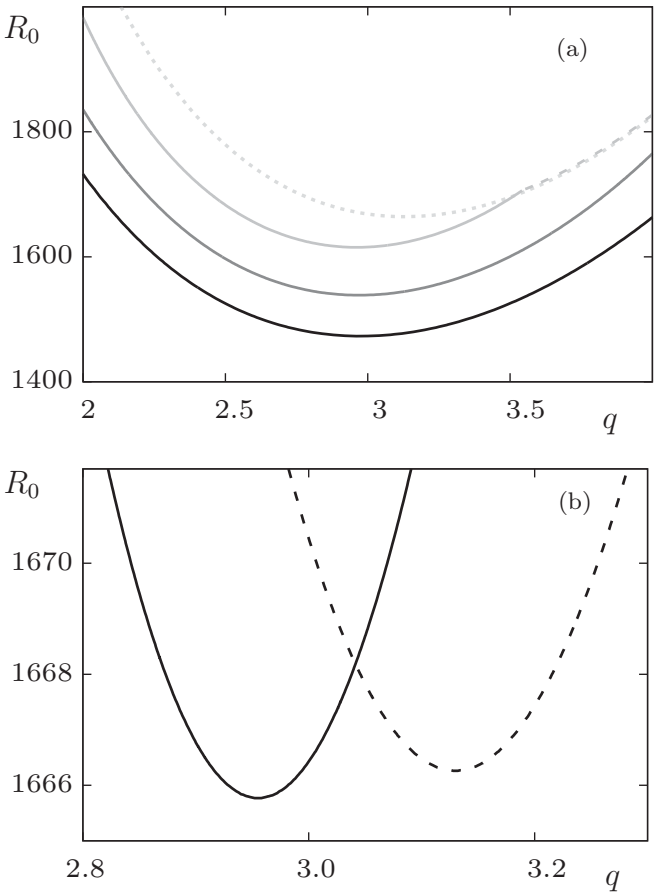

FIG. 1. Neutral curves $R_0(q)$ are shown for different values of the conductivity parameter ζ and $\psi = 10^{-5}$. Solid lines mark stationary bifurcations and dotted and dashed lines mark oscillatory ones. In part (a), one has $\zeta = 0$ (black solid line), $\zeta = 0.06$ (dark gray solid line), $\zeta = 0.08$ (gray solid and dashed lines), and $\zeta = 0.10$ (light gray dotted line). (b) Two neutral curves, which correspond to the two eigenvalues with the largest real parts, are shown at $\zeta = 0.0875$. Again, the solid line indicates a stationary bifurcation and the dashed line an oscillatory one.

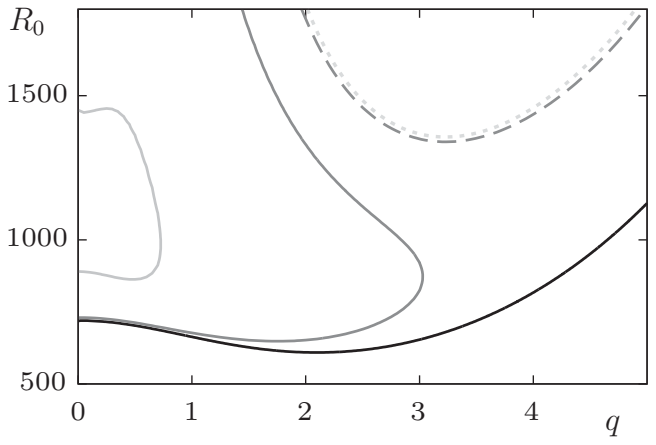

FIG. 2. Neutral curves $R_0(q)$ are shown for $\psi = 10^{-4}$ and the heat conductivity parameter $\zeta = 0$ (black solid line), $\zeta = 0.05$ (dark-gray lines), $\zeta = 0.15$ (gray solid line), and $\zeta = 0.20$ (light gray dotted line). At $\zeta = 0.05$, the neutral curve splits into the dark gray solid part for the stationary and the dark gray dashed line for the oscillatory instability. At $\zeta = 0.15$, the gray solid line marks the stationary branch and the oscillatory one is not shown. The light gray dotted line corresponds to the oscillatory instability at $\zeta = 0.20$.

We also mention for completeness that the Rayleigh number at the onset of convection in binary fluids decreases in the range of $\psi > 0$ with increasing values of ψ starting at $R_c(\psi = 0) \simeq 1708$. Simultaneously, the critical wave number q_c of the stationary bifurcation tends to zero in the range $\psi \gtrsim L$ [26,29,30].

For increasing values of ζ, the neutral curve $R_0(q)$ of the stationary bifurcation is shifted to larger values, as illustrated in Fig. 1(a). For $\zeta = 0.08$, at about $q \simeq 3.55$ along $R_0(q)$ a transition takes place from a stationary bifurcation in the range $q \leqslant 3.55$ to an oscillatory one in the range $q \gtrsim 3.55$. We mention that here, and in all following figures, solid lines mark stationary bifurcations whereas dashed, dotted, or dashed-dotted curves indicate oscillatory bifurcations. The neutral curve is determined by the condition given in Eq. (19) for the eigenvalue with the largest real part. At about $q \simeq 3.55$, the real parts of three different eigenvalues cross each other as a function of q, where the eigenvalue of the stationary bifurcation has the largest eigenvalue in the range $q \leqslant 3.55$ and a pair of complex conjugate eigenvalues leading to an oscillatory bifurcation has the largest real part in the range $q \gtrsim 3.55$. Accordingly, at the transition between the two instabilities, one has an unsteady change of the slope along the lowest neutral line. At a slightly larger value of ζ, this transition takes place at a smaller value of q and the path along the lowest parts of the two neutral curves belonging to the two instabilities becomes nonmonotonic, as illustrated in Fig. 1(b) for $\zeta = 0.0875$. At the crossing point of the two neutral curves in Fig. 1(b), the eigenvalue of the stationary branch vanishes as well as the real parts of the two complex conjugate eigenvalues at the oscillatory branch. This type of an exchange of instabilities is different from the well-known codimension-2 point in molecular binary fluids [26,29], where only two of the three eigenvalues are involved and one has a so-called double zero eigenvalue problem [31].

At larger, but still small, values of the separation ratio ψ, the transition from a stationary to a Hopf bifurcation, which occurs by increasing ζ, takes place in a different and more diverse manner, as exemplified in Fig. 2 for $\psi = 10^{-4}$. The neutral curve of the stationary bifurcation at $\zeta = 0$ (black solid line) is strongly deformed by changing ζ to $\zeta = 0.05$ (dark gray curves). The minimum of the latter curve at q_c is shifted to a smaller value compared to the black line. Moreover, for certain wave numbers, e.g., $q = 2.5$, one eigenvalue σ vanishes at two different values of R by crossing two times the dark gray solid line. Between these two values of R, the growth rate $\mathrm{Re}(\sigma)$ is positive and otherwise is negative. Beyond the dark gray solid curve at an even higher value for R at $q = 2.5$ and $\zeta = 0.05$, the real parts of a pair of complex conjugate eigenvalues change their sign and become positive, namely, beyond the dark gray dashed line. Increasing the conductivity parameter up to $\zeta = 0.15$, the gray solid line for the stationary bifurcation results, which is even further deformed compared to the case $\zeta = 0.05$. Increasing ζ beyond $\zeta = 0.15$, the stationary branch vanishes at about $\zeta = 0.165$, and beyond this value, only a Hopf bifurcation from the heat conductive state takes place as shown by the light gray dotted line for $\zeta = 0.2$. Since the value of the Rayleigh number of the neutral curves at the Hopf branch changes only slightly as a function of ζ, the Hopf branch belonging to $\zeta = 0.15$ is not shown.

This transition scenario (that increasing values of ζ lead to a growth of the critical Rayleigh number at the onset of stationary convection and finally to a Hopf bifurcation to convection at even higher Rayleigh numbers) is illustrated from a slightly different perspective by Fig. 3. In this figure, the critical values $R_c = R_0(q_c)$, q_c, and ω_c at the minimum of the lowest neutral curves are plotted as functions of the conductivity parameter ζ. The solid lines, describing the stationary bifurcation as a function of ζ, cease to exist at about $\zeta = 0.165$. During the process of disappearance of the stationary bifurcation, the neutral curve of this bifurcation is deformed, as illustrated in Fig. 2. Beyond $\zeta = 0.165$, a Hopf bifurcation from the heat conductive state is preferred. Within the oscillatory region, R_c varies only slightly with ζ and takes values that are more than 100% larger than the corresponding value for $\zeta = 0$. The critical wave number decreases initially, exhibits a major jump at the transition point, and remains finally nearly constant, taking a value of $q_c \simeq 3.2$, which is close to the critical wave number for a simple Newtonian fluid $q_c^{\mathrm{NF}} = 3.116$. The critical Hopf frequency is monotonically increasing.

A third perspective on the transition from a stationary bifurcation to a Hopf bifurcation is provided in Fig. 4 for $\zeta = 0.1$ and in Fig. 5 for $\zeta = 0.2$. In both figures, we present the critical values R_c resp. R_c, q_c, and ω_c as functions of the separation ratio ψ. As a guide to the eye, we have also included the well-known limiting case for $\zeta = 0$ (gray solid lines). Again, solid curves describe the critical values for a stationary bifurcation, if this threshold is lower than the Hopf bifurcation, and dashed lines the critical values of the Hopf bifurcation.

The left transition from a stationary bifurcation to a Hopf bifurcation in Figs. 4 and 5 is a codimension-2 bifurcation as illustrated in Fig. 1(b). The critical Rayleigh numbers at the minimum of the neutral curve of the stationary bifurcation at

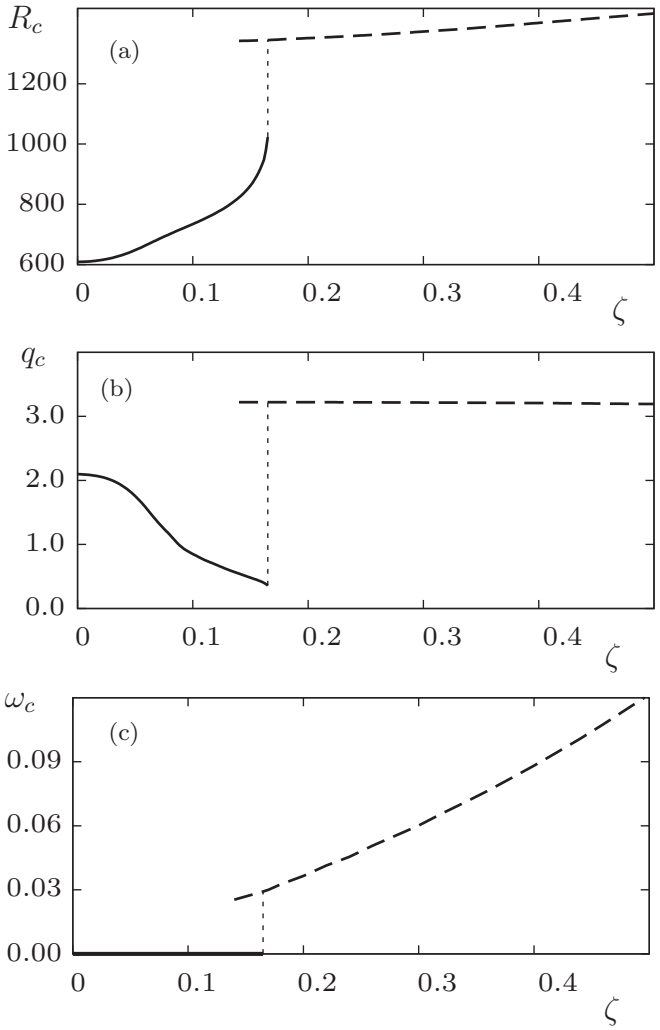

FIG. 3. Part (a) shows the critical Rayleigh number R_c, (b) shows the critical wave number q_c, and (c) shows the critical frequency ω_c as a function of ζ for $\psi = 10^{-4}$. Solid lines mark a stationary onset of convection and dashed lines mark an oscillatory one.

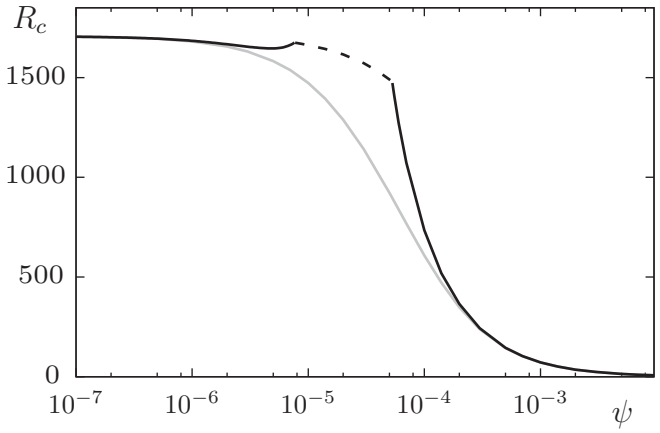

FIG. 4. The critical Rayleigh number R_c is given as a function of ψ for $\zeta = 0.0$ (gray line) and $\zeta = 0.1$ (black lines). In the latter case, the solid line marks the stationary and the dashed line the Hopf branch. At the transition from the stationary to the Hopf branch, one has a codimension-2 point.

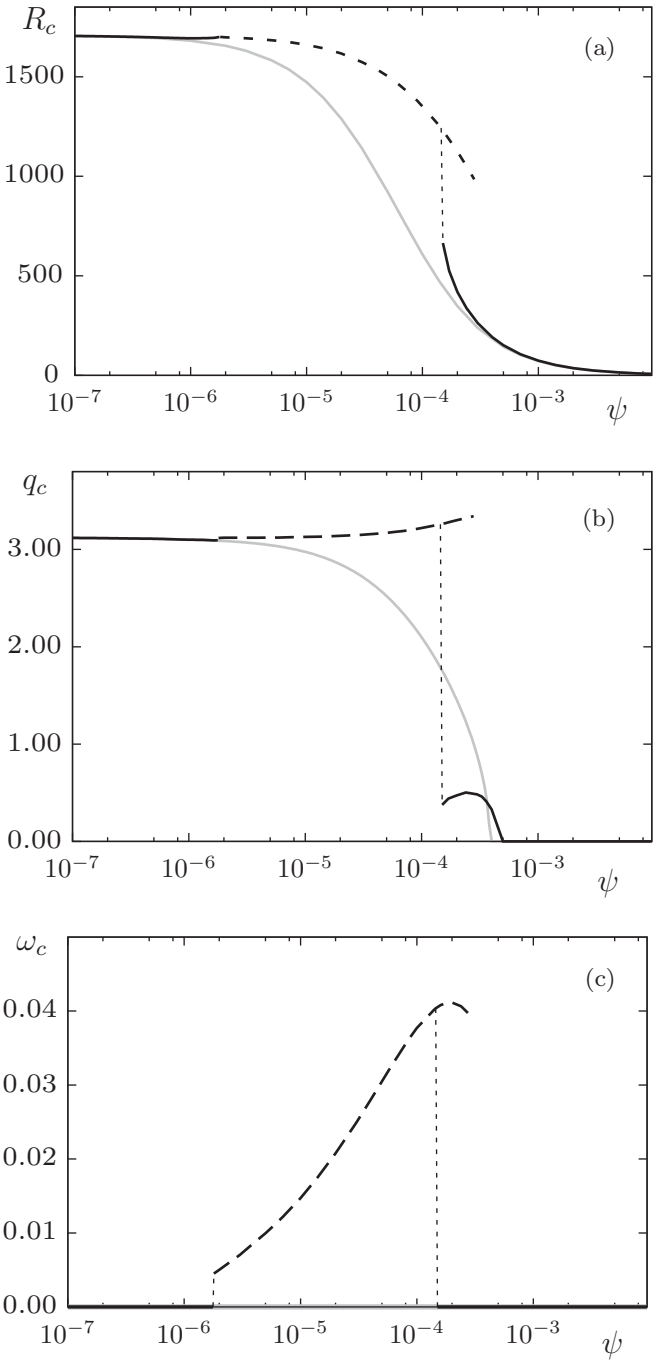

FIG. 5. In part (a), the critical Rayleigh number R_c is shown as a function of ψ for $\zeta = 0$ (gray line) and $\zeta = 0.2$ (black lines), whereby in the latter case the solid lines mark a stationary bifurcation and the dashed line a Hopf bifurcation. Part (b) shows the corresponding critical wave number $q_c(\psi)$ and part (c) shows the frequency $\omega_c(\psi)$.

q_c^S and at the minimum of the Hopf branch at q_c^H come rather close to each other with $q_c^H - q_c^S \simeq 0.025$ in Fig. 5.

With further increasing values of ψ, the transition from the Hopf branch back to a stationary branch is different for $\zeta = 0.1$ (Fig. 4) and $\zeta = 0.2$ (Fig. 5). The right transition in Fig. 4 is similar to the left one and resembles qualitatively the scenario shown in Fig. 1(b). By reducing ζ below $\zeta = 0.1$,

the two transitions shown in Fig. 4 approach each other and one obtains a rather degenerate bifurcation structure. The interesting nonlinear dynamics in this parameter range will be discussed in more detail elsewhere. The right transition in Fig. 5 shows a jump in the wave number and is in this respect rather different: By approaching this transition from larger values of ψ, the stationary branch ceases to exist (cf. Fig. 2). To the right of this second transition point, convection sets in stationary. However, with decreasing values of ψ, the stationary part of the neutral curve becomes more and more deformed [just as in the case of increasing values of ζ at a fixed ψ (cf. Fig. 2)] and finally ceases to exist at the codimension-2 point. Also, this transition with quite disparate wave numbers at the two bifurcations bears an interesting nonlinear behavior, which is to be discussed elsewhere.

The ψ range where convection sets in via a Hopf bifurcation changes as a function of the conductivity parameter ζ, as shown in Fig. 6. In the gray region within the displayed curve, we find a Hopf bifurcation to convection; outside the curve, a stationary bifurcation takes place. Close to the left nose of this curve, one has two transition points as in Fig. 4, whereas for larger values of ζ, the situation resembles the one shown in Fig. 5, with a strong jump in the wave number and the Rayleigh number along the upper part of the curve.

In the limit of a vanishing Soret effect, i.e., $\psi \to 0$, temperature gradients do not cause concentration gradients anymore, the particle concentration becomes homogeneous, and the heat diffusivity χ is independent of the temperature. In molecular binary-fluid mixtures, one has a codimension-2 point at $\psi_{\mathrm{CTP}} \simeq -L^2$, with a stationary bifurcation for $\psi > \psi_{\mathrm{CTP}}$ and a Hopf bifurcation in the range $-1 < \psi < \psi_{\mathrm{CTP}}$ [25,26,29]. In colloidal suspensions with $L \simeq 10^{-4}$ or smaller, this codimension-2 point ψ_{CTP} is even closer to zero.

In the range $\psi < \psi_{\mathrm{CTP}}$, the Soret effect causes an enhancement of the particle concentration near the lower plate and, with $\gamma > 0$, also the heat conductivity increases at this boundary. For rising values of ζ, we find a monotonous reduction of the critical Rayleigh number at the Hopf bifurcation compared to the limit $\zeta = 0$. This is an opposite trend in comparison to the enhancement of the threshold found in the range $\psi > 0$. However, this reduction of the Rayleigh number at the Hopf bifurcation is rather small and no deformation of neutral curves takes place. With increasing ζ, the critical wave number q_c decreases slightly and the frequency ω_c increases almost linearly, similar to the behavior depicted in Fig. 3(c). For example, at $\psi = -10^{-4}$ and in the range $0 \leqslant \zeta \leqslant 0.5$, R_c decreases with rising values of ζ from $R_c = 1708$ at $\zeta = 0$ to 1624 at $\zeta = 0.5$, q_c decreases from $q_c = 3.116$ to 3.097, and ω_c increases from $\omega_c = 0.19$ to 0.28.

The thermal conductivity contrast $\tilde{\kappa}$ is a function of the product $R\psi\zeta = \xi$. Since R_c keeps large values at the Hopf bifurcation with decreasing ψ, in contrast to the range $\psi > 0$ [26,29], the assumption of a linear variation of the particle concentration along the vertical z coordinate is violated at medium values of ζ, i.e., the linear dependence of the thermal conductivity on the particle concentration becomes violated for smaller values of ζ than in the range $\psi > 0$.

The symmetry breaking caused by the nonlinear ground state of the temperature and concentration field generates characteristic changes of the flow field. Let us first concentrate on the case $\psi > 0$. We found that, for nonvanishing values of ζ, the center z_0 of the convection rolls is always shifted out of the center of the cell at $z = 0$ toward the lower plate, i.e., $z_0 < 0$. For a fixed value of $\psi > 0$, the position z_0 decreases monotonically for rising values of ζ as long as the onset of convection is stationary and, besides this shift, no further qualitative deformation of the convection rolls takes place. A typical flow field for this situation is presented in Fig. 7(a) for $\psi = 10^{-5}$ and $\zeta = 0.085$, where we show contour lines of the stream function Φ. This behavior changes when ζ takes even larger values for which convection sets in via a Hopf bifurcation. In this parameter range, we find inclined convection rolls, as exemplarily presented in Fig. 7(b) for

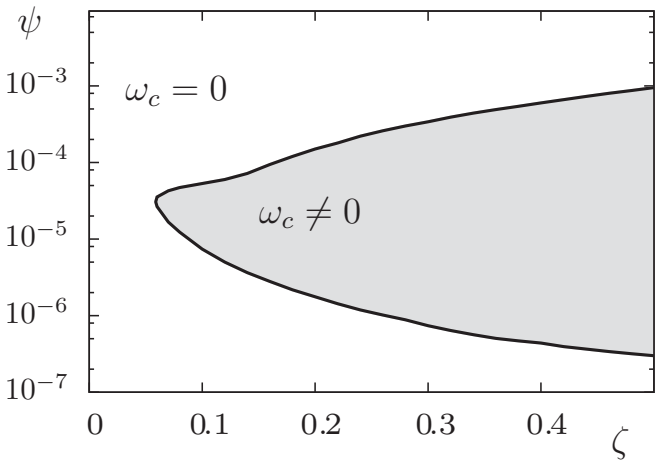

FIG. 6. Location of the two codimension-2-points (cf. Figs. 4 and 5) in the ζ-ψ plane. In the gray region inside the black curve, the onset of convection takes place via a Hopf bifurcation and otherwise via a stationary bifurcation.

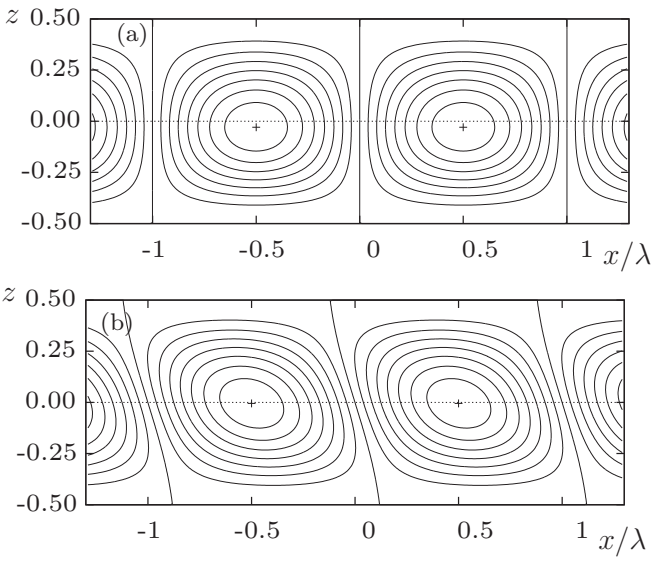

FIG. 7. Contour lines of the stream function Φ at the onset of convection for (a) $\psi = 10^{-5}$ and $\zeta = 0.085$ (stationary instability) and for (b) $\Psi = 10^{-4}$ and $\zeta = 0.3$ (oscillatory instability). The center of the convection rolls is shifted to $z_0 = -0.029$ and -0.005, respectively. Here, $\lambda = \pi/q_c$.

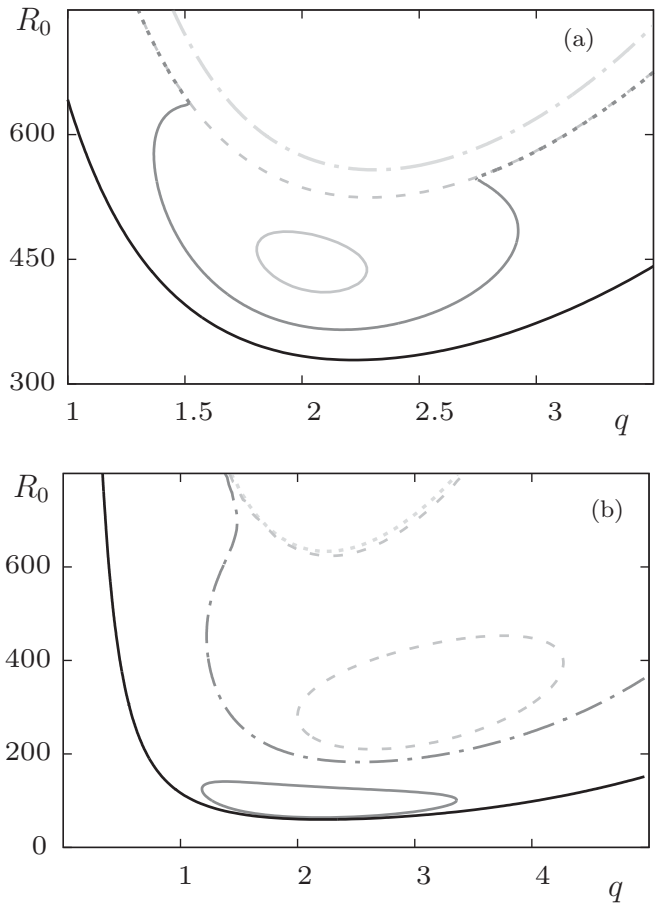

FIG. 8. Neutral curves $R_0(q)$ for different values of the conductivity parameter ζ are shown in part (a) at $\psi = 10^{-4}$ with $\zeta = 0$ (black solid line), $\zeta = 0.08$ (dark gray lines), $\zeta = 0.095$ (gray lines), and $\zeta = 0.50$ (light gray dashed-dotted line) and in part (b) at $\psi = 10^{-3}$ with $\zeta = 0$ (black solid line), $\zeta = 0.20$ (dark gray lines), $\zeta = 0.35$ (gray lines), and $\zeta = 0.50$ (light gray dotted line). Solid curves mark stationary instabilities and all other line types mark oscillatory ones.

$\psi = 10^{-5}$ and $\zeta = 0.30$. Left traveling waves (LTW, with $\omega_c > 0$) are inclined to the left, right traveling waves (RTW, with $\omega_c < 0$) are inclined to the right. Similarly, inclined rolls appear also for negative values of the separation ratio and finite values of ζ but, in contrast to the results for $\psi > 0$, the center is slightly shifted toward the upper boundary for $\psi < 0$.

The dependence of the shift of the center of the convection rolls on the sign of the separation ratio ψ can be understood as follows. For $\psi > 0$, the suspended particles are driven to the upper plate of the convection cell and, hence, the thermal conductivity rises from the lower to the upper plate. As the vertical heat current $j_z = -\chi \partial_z T_{\text{cond}}$ is independent of z [compare Eq. (8)], it follows straightforwardly that the gradient of the temperature profile, which enhances the onset of convection, decreases from the lower to the upper plate. Therefore, the fluid motion tends to concentrate in the region of the lower boundary, which results into a shift of the center of the convection rolls to $z_0 < 0$. Obviously, the situation is reversed for $\psi < 0$ and, hence, the center of convection rolls is shifted upward.

B. Free-slip, permeable boundary conditions

Let us now turn to free-slip, permeable boundary conditions. It is well known that, for free-slip, permeable boundary conditions (16) instead of no-slip, impermeable boundary conditions (15), the critical wave number q_c does not tend to zero for increasing values of ψ [26,29]. Despite this difference, the major trends are similar. For finite values of ζ, the threshold is enhanced compared to its value at $\zeta = 0$ in the range $\psi > 0$ and lowered in the range $\psi < 0$. As in the case of no-slip, impermeable boundary conditions, we find a competition between a stationary and an oscillatory onset of convection in the range $\psi > 0$, which, however, reveals some differences, as described in this section.

Figure 8 shows neutral curves for different values of ζ at $\psi = 10^{-4}$ and 10^{-3}. For smaller values of the separation ratio, the major effect of finite values of ζ is a shift toward higher Rayleigh numbers, very similar to the situation depicted in Fig. 1(a). For $\psi = 10^{-4}$, the neutral curves are additionally deformed and split into a stationary branch and an oscillatory branch at higher Rayleigh numbers, as illustrated in Fig. 8(a). Even though the situation is similar to the one shown in Fig. 2, there are some interesting differences. For $\zeta = 0.08$, the dark gray solid curve merges with the dark gray dotted curve without crossing, i.e., two stationary eigenvalues merge and build a pair of complex conjugate ones similar to those presented in Fig. 9 for $\zeta = 0.095$. The island at finite values of q marked by the gray solid curve in Fig. 8(a) and corresponding to $\zeta = 0.095$ is a further feature that differs from the case of no-slip boundary conditions. The upper boundary of this curve marks a linear restabilization of the heat conductive state, as indicated by the second sign change of the real part in Fig. 9. After the restabilization, an even higher positioned Hopf bifurcation occurs, as described by the gray dashed line in Fig. 8(a), which in the ranges of small and large values of q almost coincides with the oscillatory branch for $\zeta = 0.08$. As this restabilization takes place far beyond the first instability, where the nonlinear contributions to the equations of motion determine the dynamics of the system, an answer to the question as to whether this restabilization is of relevance for a real system can only be given by solving the nonlinear equations of motion in that range.

For separation ratios larger than $\psi = 10^{-4}$, even a linear restabilization of the oscillatory bifurcation may occur. This is illustrated for $\psi = 10^{-3}$ in Fig. 8(b). For $\zeta = 0.2$, we find a linear restabilization of the stationary branch, as depicted by the dark gray solid line, before an oscillatory bifurcation from the heat conductive state (dark gray dashed-dotted line) takes place. In contrast, for larger values of ζ, e.g., $\zeta = 0.35$, the stationary branch has already disappeared and the lowest instability is given by a Hopf bifurcation. Here, this oscillatory branch shows a linear restabilization and a second Hopf bifurcation arises at even higher values of R as shown by the upper gray dashed curve in Fig. 8(b).

These interesting bifurcation scenarios, including two exchanges of instabilities, are presented from a different perspective in Fig. 10. Here, the critical values R_c, q_c, and ω_c are shown as functions of ζ. In the first coexistence range, the situation is similar to the case of rigid boundary conditions, i.e., the end point of the solid line corresponds to the disappearance

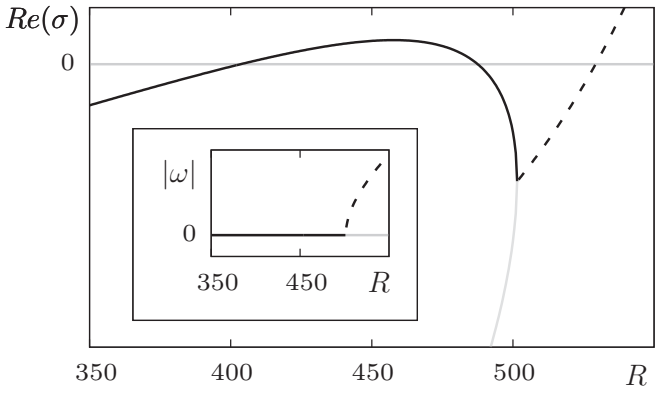

FIG. 9. The real parts of the two largest eigenvalues are shown as functions of the Rayleigh number R corresponding to the neutral curves in Fig. 8(a) for $\zeta = 0.095$ and at $q = q_c \simeq 2.1$. The black solid line marks the stationary branch and has two zero crossings, which define the boundary of the closed curve in Fig. 8(a). At about $R \simeq 502$, this real eigenvalue merges with a second real eigenvalue (light gray solid line) to a pair of complex conjugate eigenvalues (black dashed line). The appendant imaginary part $|\omega|$ is depicted in the inset.

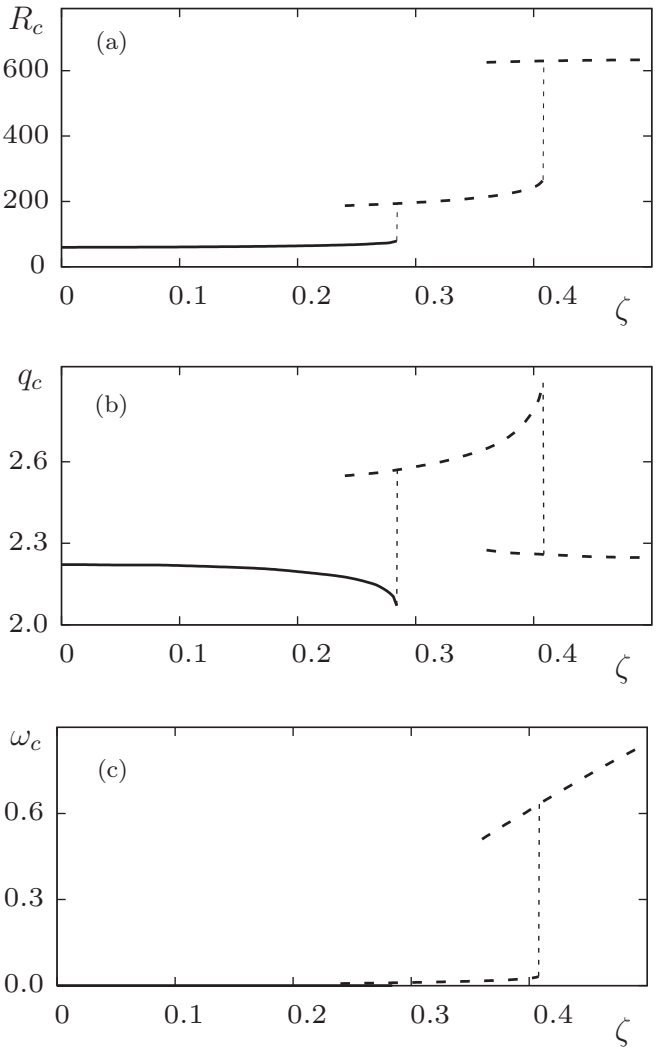

FIG. 10. The critical Rayleigh number R_c in (a), the critical wave number q_c in (b), and the critical frequency ω_c in (c) are shown as functions of ζ for $\psi = 10^{-3}$. Solid lines mark a stationary onset of convection and dashed lines mark an oscillatory one.

of an isolalike deformed stationary neutral curve. Similarly, in the second coexistence range, the first oscillatory instability ceases to exist at the end point of the dashed line, leaving behind a second oscillatory instability at even higher values of the Rayleigh number. We mention that, unlike the end points of the solid and first dashed line, the starting points of both dashed lines are not related to the creation or aniquilation of isolas. We decided to display these lines also to the left of the transition points to stress the fact that the oscillatory branches are already present before another branch vanishes (cf. Fig. 8). The critical wave numbers and frequencies corresponding to the three distinct instabilities differ considerably.

A further illustration of the bifurcation scenario is given by Fig. 11, where the critical Rayleigh number R_c and the critical wave number q_c are shown as functions of the separation ratio ψ for a conductivity parameter of $\zeta = 0.2$. Again, we find the most pronounced changes in comparison to $\zeta = 0$ in the range $\psi \sim L = 10^{-4}$. When the two codimension-2 points marking the exchange of instabilities are plotted as functions of ζ, the resulting curve shows a similar behavior as the one for no-slip boundary conditions in Fig. 6.

In accordance with the results for no-slip boundary conditions, one obtains for negative values of the separation ratio ψ and finite values of ζ a reduction of the threshold compared to the case $\zeta = 0$. The critical wave number is independent from ζ and takes the value $q_c = \pi/\sqrt{2}$, just as in the case of molecular binary-fluid mixtures.

For finite values of ζ, the changes in the flow field at the onset of convection with respect to the limiting case $\zeta = 0$ are qualitatively very similar to those discussed for no-slip boundary conditions. While a positive separation ratio $\psi > 0$ lowers the center of convection rolls, the opposite happens in the case $\psi < 0$. In addition, an oscillatory onset leads to inclined rolls. As for free-slip boundary conditions, the velocity field takes finite values at both plates, and the shift of the center is larger than in the case of no-slip boundary conditions.

IV. DISCUSSION AND CONCLUSION

The onset of thermal convection in a colloidal suspension was investigated by means of a generalized continuum model for binary-fluid mixtures, which has been extended beyond the Boussinesq approximation by taking into account a linear dependence of the thermal conductivity on the local concentration of colloidal particles.

We investigated colloidal suspensions where the thermal conductivity of the suspension increases with rising values of the particle concentration. An inhomogeneous particle concentration can be induced by temperature variations via the Soret effect, which corresponds to finite values of the separation ratio ψ. The concentration-dependent thermal conductivity causes a nonlinear variation of the temperature across the convection cell, in contrast to a linear variation for a constant thermal

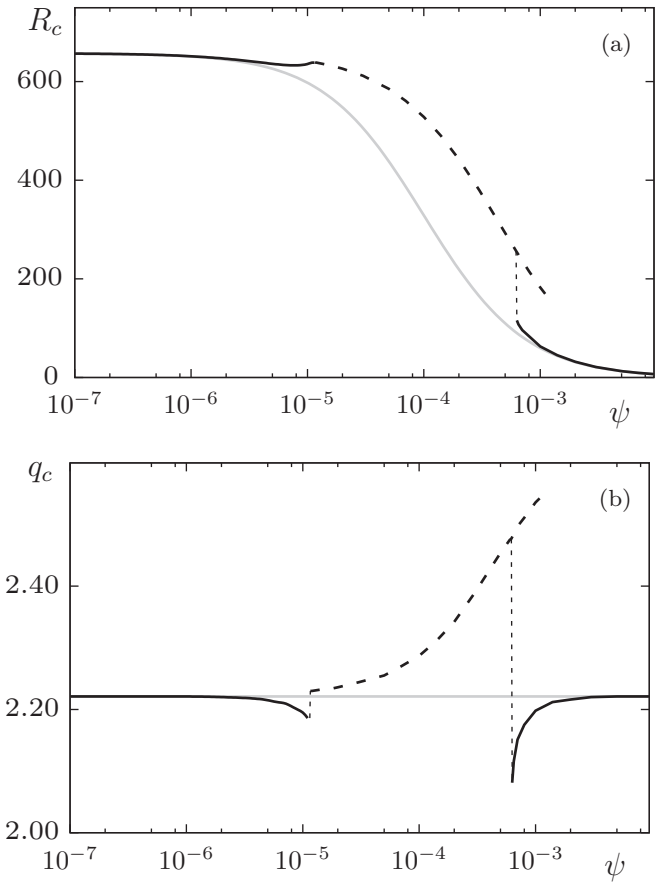

FIG. 11. Part (a) shows the critical Rayleigh number R_c as a function of the separation ratio ψ for $\zeta = 0$ (gray solid line) and $\zeta = 0.2$ (black lines), where, in the latter case, the solid lines mark the stationary branch and the dashed line marks the oscillatory one. Part (b) shows the corresponding critical wave number q_c using the same line styles.

conductivity. The strength of the spatial variations of the heat conductivity is described by a dimensionless heat conductivity parameter ζ, as introduced in this paper. It was found that, for finite values of ζ, the vertical heat current through the convection cell is reduced compared to the case of a constant heat conductivity.

For positive values of the separation ratio ψ, the suspended particles are driven to the colder upper plate of the convection cell, and for a constant heat conductivity, i.e., $\zeta = 0$, a stationary bifurcation from the heat conductive state to convection takes place. Spatial variations of the heat conduction, corresponding to $\zeta \neq 0$, lead to a shift of the critical Rayleigh number R_c to larger values than obtained in the case $\zeta = 0$. Additionally, beyond some critical value ζ_c and in the parameter range $\psi \sim L$, the onset of convection takes place via a Hopf bifurcation. This trend (i.e., that a delay of the onset of convection leads to a Hopf bifurcation) is also met in the range $\psi < 0$, and is well known from molecular binary-fluid mixtures.

Vertical variations of material properties, as discussed in this paper for the thermal conductivity, are considered to be important for modeling convection in the Earth's mantle and, accordingly, a number of models including non-Boussinesq effects were explored [1,18]. For modeling convection in systems with spatially varying material parameters, two superimposed layers of immiscible [49–51] or even miscible fluids [52] are also used. As in our system, with its spatially varying heat conductivity, an oscillatory onset of convection was found in such two-layer systems for various parameters.

The range of positive ψ values, where the Hopf bifurcation takes place, increases with rising values of ζ. At both boundaries of this range, we find a codimension-2 bifurcation, where the thresholds of the stationary and the oscillatory bifurcations coincide. Additionally, one has a further codimension-2 bifurcation at $\psi \lesssim 0$, which is well known from earlier investigations of molecular binary-fluid mixtures. However, for no-slip boundary conditions, the two codimension-2 points occurring for $\psi > 0$ are qualitatively different. Here, the two neutral curves belonging to the two different bifurcations cross each other and, therefore, three eigenvalues are close to be critical. In contrast to this, only two eigenvalues are critical close to the codimension-2 bifurcation at $\psi \lesssim 0$. At the left boundary of the ψ range, where a Hopf bifurcation is preferred, one encounters usually small jumps in the critical wave number, whereas large jumps occur at the right boundary of this range.

During our analysis, we assumed $\gamma > 0$ in Eq. (1), corresponding to the situation wherein the thermal conductivity of the particles is higher than the one of the base fluid. Hence, the local heat conductivity increases with a rising particle concentration. However, we obtain for $\gamma < 0$ exactly the same bifurcation scenarios as described in this paper for $\gamma > 0$. This may be understood as follows. Independent of the sign of γ, one obtains in the presence of thermophoresis layers of higher and lower thermal conductivity accompanied by a nonlinear z dependence of the temperature. Changing the sign of γ changes both the variation of the heat conduction and the temperature profile, but the vertical heat current is identical for both signs of γ, as indicated by Eq. (8).

A further interesting question is how a spatially varying heat conductivity affects the ratio between the convective and conductive heat transfer (Nusselt number) beyond the onset of convection, and how to understand the effects of boundary layers with enhanced or reduced heat conductivity.

ACKNOWLEDGMENTS

Stimulating discussions with F. H. Busse, M. Evonuk, G. Freund, W. Pesch, I. Rehberg, and W. Schöpf are appreciated. This work was supported by the German Science Foundation through the research unit FOR 608.

APPENDIX: DETERMINATION OF THE HEAT CONDUCTIVE STATE

In the heat conductive state, i.e., $\mathbf{v} = 0$, the temperature distribution $T_{\mathrm{cond}}(z)$ and the particle distribution $N_{\mathrm{cond}}(z)$ are

determined by the two equations

$$0 = \partial_z\{[1+\gamma(N_{\rm cond}-N_0)]\partial_z T_{\rm cond}\}\,, \tag{A1a}$$

$$0 = \partial_z^2 N_{\rm cond} + \frac{k_T}{T_0}\,\partial_z^2 T_{\rm cond}\,. \tag{A1b}$$

For a vanishing mass current at the boundaries [cf. Eq. (4b)], a double integration of Eq. (A1b) yields

$$N_{\rm cond} = -\frac{k_T}{T_0}\,T_{\rm cond} + N_0 + n_0\,. \tag{A2}$$

Now, Eq. (A1a) takes the form

$$0 = \partial_z^2\left((1+\gamma n_0)\,T_{\rm cond} - \frac{k_T}{2T_0}T_{\rm cond}^2\right) \tag{A3}$$

and its integration gives

$$T_{\rm cond}^2 - \Gamma_0\,T_{\rm cond} = \tfrac{1}{4}(C_1\,z + C_0)\,, \tag{A4}$$

with $\Gamma_0 = (1+\gamma n_0)T_0/(\gamma k_T)$. Solving this quadratic equation, the two unknown constants C_0 and C_1 are determined by the two boundary conditions (4a) for $T_{\rm cond}$ and one obtains

$$T_{\rm cond} = \Gamma_0 - \sqrt{M_+^2\left(\frac{1}{2}-\frac{z}{d}\right) + M_-^2\left(\frac{1}{2}+\frac{z}{d}\right)}\,, \tag{A5}$$

with $M_\pm = \Gamma_0 + T_0 \pm \delta T/2$. The last free constant n_0 in Eq. (A2) is determined by the definition of N_0:

$$N_0 = \frac{1}{d}\int_{-d/2}^{d/2} N_{\rm cond}\,dz = N_0 + n_0 - \frac{k_T}{T_0 d}\int_{-d/2}^{d/2} T_{\rm cond}\,dz\,. \tag{A6}$$

[1] *Mantle Dynamics*, Treatise on Geophysics, Vol. 7, edited by D. Bercovici (Elsevier, Amsterdam, 2009).
[2] F. H. Busse, in *Mantle Convection: Plate Tectonics and Global Dynamics*, edited by W. R. Peltier (Gordon and Breach, New York, 1989).
[3] R. A. Houze, *Cloud Dynamics* (Academic, San Diego, 1993).
[4] J. A. Eastman, S. R. Phillpot, S. U. S. Choi, and P. Keblinski, Annu. Rev. Mater. Res. **34**, 219 (2004).
[5] J. Buongiorno, J. Heat Transfer **128**, 240 (2006).
[6] J. Buongiorno *et al.*, J. Appl. Phys. **106**, 094312 (2009).
[7] S. U. S. Choi, J. Heat Transfer **131**, 033106 (2009).
[8] M. C. Cross and P. C. Hohenberg, Rev. Mod. Phys. **65**, 851 (1993).
[9] E. Bodenschatz, W. Pesch, and G. Ahlers, Annu. Rev. Fluid Mech. **32**, 709 (2000).
[10] M. C. Cross and H. Greenside, *Pattern Formation and Dynamics in Nonequilibrium Systems* (Cambridge University Press, Cambridge, 2009).
[11] F. H. Busse, J. Fluid Mech. **30**, 625 (1967).
[12] E. Palm, J. Fluid Mech. **8**, 183 (1960).
[13] K. E. Torrance and D. L. Turcotte, J. Fluid Mech. **47**, 113 (1971).
[14] F. H. Busse and H. Frick, J. Fluid Mech. **150**, 451 (1985).
[15] U. R. Christensen and H. Harder, Geophys. J. Int. **104**, 213 (1991).
[16] S. Balachandar, D. A. Yuen, D. M. Reuteler, and G. S. Lauer, Science **267**, 1150 (1995).
[17] M. Ogawa, Fluid Dyn. Res. **40**, 379 (2008).
[18] A. P. van den Berg, D. A. Yuen, and V. Steinbach, Geophys. Res. Lett. **28**, 875 (2001).
[19] S. J. Linz and M. Lücke, Phys. Rev. A **36**, 3505 (1987).
[20] B. Huke, H. Pleiner, and M. Lücke, Phys. Rev. E **78**, 046315 (2008).
[21] M. Glässl, M. Hilt, and W. Zimmermann, Eur. Phys. J. E **32**, 265 (2010).
[22] J. K. Platten and L. C. Legros, *Convection in Liquids* (Springer, Berlin, 1984).
[23] J. S. Turner, Annu. Rev. Fluid Mech. **17**, 11 (1985).
[24] L. D. Landau and E. M. Lifschitz, *Fluid Mechanics*, Course of Theoretical Physics, Vol. 6 (Butterworth, Boston, 1987).
[25] H. R. Brand, P. C. Hohenberg, and V. Steinberg, Phys. Rev. A **30**, 2548 (1984).
[26] M. C. Cross and K. Kim, Phys. Rev. A **37**, 3909 (1988).
[27] E. Knobloch and D. R. Moore, Phys. Rev. A **37**, 860 (1988).
[28] W. Schöpf and W. Zimmermann, Europhys. Lett. **8**, 41 (1989).
[29] W. Schöpf and W. Zimmermann, Phys. Rev. E **47**, 1739 (1993).
[30] M. Lücke *et al.*, in *Evolution of Spontaneous Structures in Dissipative Continuous Systems*, edited by F. H. Busse and S. C. Müller (Springer, Berlin, 1998).
[31] J. Guckenheimer and P. Holmes, *Nonlinear Oscillations, Dynamical Systems, and Bifurcations of Vector Fields* (Springer, New York, 1983).
[32] R. Cerbino, A. Vailati, and M. Giglio, Phys. Rev. E **66**, 055301 (2002).
[33] R. Cerbino, S. Mazzoni, A. Vailati, and M. Giglio, Phys. Rev. Lett. **94**, 064501 (2005).
[34] M. C. Kim, C. K. Choi, and J.-K. Yeo, Phys. Fluids **19**, 084103 (2007).
[35] G. Donzelli, R. Cerbino, and A. Vailati, Phys. Rev. Lett. **102**, 104503 (2009).
[36] F. Winkel *et al.*, New J. Phys. **12**, 053003 (2010).
[37] S. K. Das, N. Putra, P. Thiesen, and W. Roetzel, J. Heat Transfer **125**, 567 (2003).
[38] R. Prasher, P. Bhattacharya, and P. E. Phelan, Phys. Rev. Lett. **94**, 025901 (2005).
[39] J. Eapen, R. Rusconi, R. Piazza, and S. Yip, J. Heat Transfer **132**, 102402 (2010).
[40] B. Huke, H. Pleiner, and M. Lücke, Phys. Rev. E **75**, 036203 (2007).
[41] D. A. Nield and A. V. Kuznetsov, Eur. J. Mech. B **29**, 217 (2010).
[42] D. Guthkowicz-Krusin, M. A. Collins, and J. Ross, Phys. Fluids **22**, 1443 (1979).
[43] G. Z. Gershuni and E. M. Zhukhovitskii, *Convective Stability of Incompressible Fluids* (Keter, Jerusalem, 1976).
[44] M. Ogawa, G. Schubert, and A. Zebib, J. Fluid Mech. **233**, 299 (1991).
[45] W. Pesch, Chaos **6**, 348 (1996).
[46] R. M. Clever and F. H. Busse, J. Fluid Mech. **65**, 625 (1974).

[47] C. Canuto, M. Y. Hassaini, A. Quarteroni, and T. A. Zang, *Spectral Methods in Fluid Dynamics* (Springer, Berlin, 1987).

[48] R. Piazza and A. Parola, J. Phys. Condens. Matter **20**, 153102 (2008).

[49] Y. Renardy and D. D. Joseph, Phys. Fluids **28**, 788 (1985).

[50] S. Rasenat, F. H. Busse, and I. Rehberg, J. Fluid Mech. **199**, 519 (1989).

[51] M. M. Degen, P. W. Colovas, and C. D. Andereck, Phys. Rev. E **57**, 6647 (1998).

[52] M. Le Bars and A. Davaille, J. Fluid Mech. **471**, 339 (2002).